SANDIA REPORT
SAND2018-12977
Printed October 2018

Head Impact from Falling Payload of a Small Balloon

Chad B. Hovey, Ryan J. Terpsma, Ramon C. Reyes, Daniel C. Bowman

Prepared by
Sandia National Laboratories
Albuquerque, New Mexico
87185 and Livermore,
California 94550

Issued by Sandia National Laboratories, operated for the United States Department of Energy by National Technology & Engineering Solutions of Sandia, LLC.

ABSTRACT

Despite the increasing number of small scientific balloon missions with payloads in the gram-to-kilogram mass range, little is known about the injury risk they pose to humans on the ground. We investigated the risk of head injury using the head injury criterion (HIC) from impact with a 1.54 kg (3.40 pound) payload. Study parameters were impact speeds of 670, 1341, and 2012 cm s^{-1} (15, 30, and 45 mph) and protective padding wall thicknesses between zero and 10 cm (3.9 inch). Padding provided meaningful reductions of injury risk outcomes at all speeds. The maximum risk of AIS 3+ injury was approximately 3.6% (HIC 249) for the 670 cm s^{-1} (15 mph) case with 0.5 cm (0.2 inch) of padding, 34% (HIC 801) for the 1341 cm s^{-1} (30 mph) case with 3.0 cm (1.2 inch) of padding, and 67% (HIC 1147) for the 2012 cm s^{-1} (45 mph) case with 7.0 cm (2.8 inch) of padding. Adding 1.0 cm (0.39 inch) of padding to these two latter cases reduced AIS 3+ injury risk to approximately 13% (HIC 498) and 37% (HIC 835), respectively. Public safety can be increased when balloon operators use padded payload enclosures as adjuncts to parachutes.

KEY TERMS: head injury criterion (HIC), expanded polystyrene padding, injury risk, balloons

ACKNOWLEDGEMENTS

We gratefully acknowledge the financial support of Sandia National Laboratories, Environment Safety & Health Planning, and John E. Myers, Safety Basis Engineer. We acknowledge Douglas Dederman for his participation in the R&A process.

CONTENTS

LIST OF FIGURES

LIST OF TABLES

This page left blank

This page left blank

ACRONYMS AND DEFINITIONS

Abbreviation	Definition
AIS	abbreviated injury scale
EOS	equation of state
EPS	expanded polystyrene
HIC	head injury criterion
NASA	National Aeronautics and Space Administration
UAS	unmanned aircraft systems

1. INTRODUCTION

Documented use of balloons in science dates to the end of the 19th century, with discovery of the two proximate layers of the Earth's atmosphere, the troposphere and stratosphere, by French meteorologist Léon Teisserenc de Bort.[17] Modern-day use of high altitude balloons has proved to be indispensable in areas of atmospheric science, heliophysics, astronomy, planetary science, and geophysics. The NASA Eclipse Ballooning Project[14] and Google Project Loon[8] are two recent well-publicized examples.

Modern balloons range in size from 2 meters (6.6 feet) diameter for standard weather balloons up to the size of an American football field, 91.4 meters (100 yards), for large scientific applications.[20]

Current balloon launch frequency ranges from several dozen launches per year for large balloon flights up to 1600 launches per day for weather balloons supporting numerical weather prediction models.[7]

In the United States, unmanned free balloons are governed by the Code of Federal Regulations Title 14, Part 101,[4] which states that balloons must not create a hazard to persons or property not associated with the operation. Large balloons must have two independent means of flight termination and produce position reports every two hours. Smaller balloons fall under an exemption that eliminates these requirements. No tracking, payload descent mechanism (parachutes, for example), or flight path restrictions are set forth for these balloons so long as

1. each payload box weighs less than 1.8 kg (4 pound) or 2.7 kg (6 pound) if the area density of the object does not exceed 13.2 g cm^{-2} (3 ounce in^{-2}),
2. the combined weight of the payload boxes does not exceed 5.4 kg (12 pound), and
3. an impact force of 22.7 kg (50 pound) or greater is sufficient to detach the payload from the balloon.

Balloon payloads typically return to Earth under a parachute to reduce impact speed. If the parachute fails to deploy correctly, payloads can strike the ground at speeds much higher than intended. The uncontrolled fall of large balloon payloads has occurred several times over the United States, most recently in 2017.[5]

The frequency and severity of high velocity impacts by smaller balloon payloads is difficult to assess due to lack of reported incidents. One known report described a prototype solar hot air balloon, which experienced an in-flight failure in 2015. The 0.8 kg (1.8 pound) science package separated from the balloon envelope at approximately 22 km (72,179 feet) altitude, and eight minutes later, struck the ground at approximately 94 km h^{-1} (58 mph). The package landed in an open field of dirt and vegetation, absent of people and property.[2]

We have been unable to find any credible reports of injury or property damage from subkilogram- (< 2.2 pound) to kilogram- (2.2 pound) scale balloon payloads such as those fielded by meteorological agencies or the amateur community. Perhaps because of this, the consequence of a small balloon payload strike to persons on the ground has not been assessed.

The objective of this study was to quantify injury risk to the head using the head injury criterion (HIC) for a range of anticipated payload impact speeds and for a range of wall thicknesses of the protective expanded polystyrene (EPS) padding payload enclosure. This analysis offers guidance to balloonists, who specify balloon payload designs and fly balloons over population centers and thus need to quantify injury risk exposure to humans from falling balloon payloads.

2. MATERIALS AND METHODS

Two assemblies, the **impactor** and the **target**, composed the geometric description of our model. The impactor, the payload carried by the balloon, was composed of an aluminum core (**instrumentation**) surrounded by an expanded polystyrene shell (**padding**). The target was human **head and neck**, composed of three layers: **brain and spinal cord**, **skull and neck**, and **skin and muscles**.

The geometry of the aluminum **instrumentation** was modeled as a right, circular cylinder 4.50 cm (1.77 inch) in radius and 8.99 cm (3.54 inch) in height. The total volume of the aluminum cylinder was 571 cm^3 (34.8 $inch^3$). The volume of the aluminum was constant for all simulations.

The geometry of the **padding** was modeled as a right, circular cylinder of varying radius and height to encase the aluminum with a constant wall thickness, parameterized from zero to 10 cm (3.9 inch). For example, in the 2 cm (0.79 inch) padding thickness case, the padding had a radius of 6.50 cm (2.56 inch) and a height of 12.99 cm (5.11 inch). The total volume of the padding was 1,151 cm^3 (70.2 $inch^3$), 1,722 cm^3 (105 $inch^3$) less the 571 cm^3 (34.8 $inch^3$) internal volume occupied by the aluminum.

The volume of the human target was created to approximate a 50th percentile American male. The total volume of the **head and neck** was 2,980 cm^3 (182 $inch^3$), composed of the following three component volumes:

- The volume for the **brain and spinal cord** was 1,408 cm^3 (85.9 $inch^3$).
- The volume for the **skull and neck** was 584 cm^3 (35.6 $inch^3$).
- The volume for the **skin and muscles** was 988 cm^3 (60.3 $inch^3$).

Figure 1-1 shows the initial positions of the **impactor** and **target**, with a midline sagittal cross-sectional view. Note that this figure shows the 2 cm (0.79 inch) padding case. The X-axis is lateral, and symmetric to the out-of-plane Z-axis. The vertical Y-axis increases from inferior to superior. The aluminum is shown in green, padding in blue, skin and muscles in yellow, head and neck in green, and brain and spinal cord in gray.

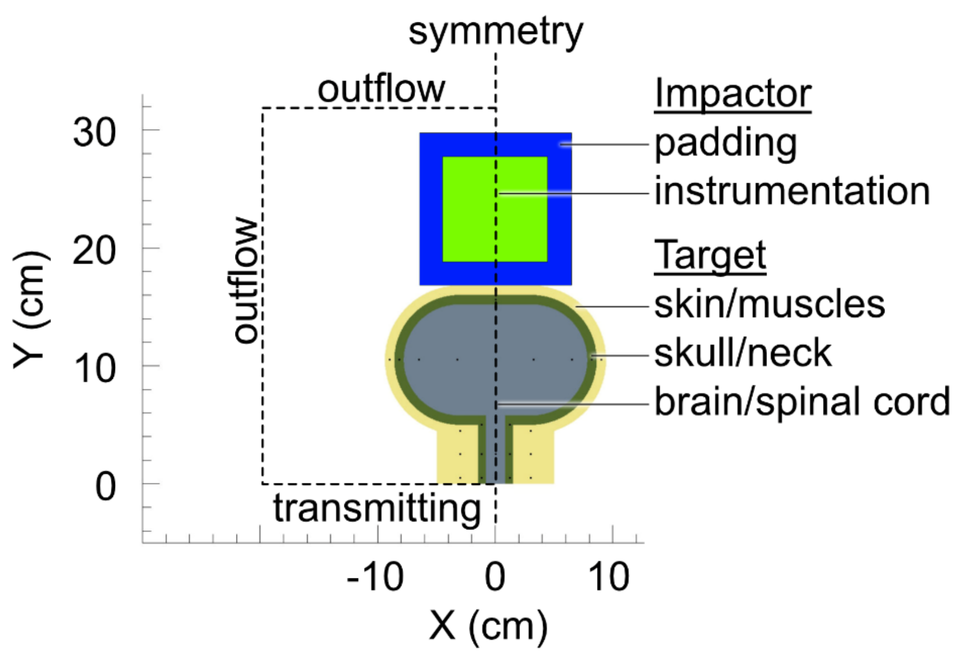

Figure 2-1. Geometry and initial configuration of the impactor and target, in midline sagittal cross-section. Symmetry, outflow, and transmitting boundary conditions are indicated.

The component materials were aluminum, expanded polystyrene, **brain and spinal cord** (white/gray matter), **skull and neck** (bone), and **skin and muscles** (soft tissue), as shown in Table 2-1.

Table 2-1. Material name and constitutive model used to characterize impactor and target.

	geometry	material	constitutive model	
			volumetric	deviatoric
impactor	instrumentation	aluminum	Sesame	Johnson-Cook
	padding	expanded polystyrene	SwRI Foam	Johnson-Cook
target	brain and spinal cord	white/gray matter	Mie-Grüneison	viscoelastic-viscoplastic
	skull and neck	bone	Mie-Grüneison	elastic perfectly plastic
	skin and muscle	soft tissue	Mie-Grüneison	elastic perfectly plastic

The stress response functions were decomposed into volumetric and deviatoric (isochoric) components.

The volumetric behavior of the aluminum used a Sesame equation of state (EOS).[13] The volumetric behavior of the padding used the SwRI EOS,[19] which captured the initial elastic region, followed by elastic pore crushing, followed by a final nonlinear hardening state. The biological volumetric behaviors used a Mie-Grüneison EOS.[9]

The deviatoric behaviors of the aluminum and padding used a Johnson-Cook strength model,[11] of bone and soft tissue used the classical elastic perfectly plastic von Mises yield surface model, and of white/gray matter used a viscoelastic-viscoplastic model.[15]

Table 2-2 lists material properties used for the impactor. Table 2-3 lists material properties used for the target. Our laboratory's previous work detailed the suitability of these models to simulate response of biological materials.[18]

Table 2-2. Material properties for the impactor.

	aluminum	expanded polystyrene
density	2.70 g cc^{-1} (0.0975 lb in^{-3})	0.0384 g cc^{-1} (0.00139 lb in^{-3})
bulk modulus	71.8 GPa (1.04e+7 psi)	8.0 MPa (1160 psi)
yield stress	324 MPa (4.70e+4 psi)	0.920 MPa (133 psi)
Poisson ratio	0.33	0.20

Table 2-3. Material properties for the target.

	soft tissue	bone	white/gray matter
density	1.20 g cc^{-1} (0.0434 lb in^{-3})	1.21 g cc^{-1} (0.0437 lb in^{-3})	1.04 g cc^{-1} (0.038 lb in^{-3})
bulk modulus	34.8 MPa (5050 psi)	4.76 GPa (6.90e+5 psi)	2.37 GPa (3.44e+5 psi)
yield stress	-	95.0 MPa (1.38e+4 psi)	-
Poisson ratio	0.42	0.22	0.49
viscosity	-	-	0.690 kPa sec (0.100 psi sec)

The total mass of the impactor varied, depending on the thickness of the padding. For all impactors, the total mass for the aluminum was 1.54 kg (3.40 pound). In the 2 cm (0.79 inch) padding thickness case, for example, the total mass of the padding was 44.3 gram (0.0977 pound). In the thickest padding case of 10 cm (3.94 inch), the padding mass was 714 gram (1.57 pound), making the most massive impactor have a total mass of 2.25 kg (4.96 pound).

The total mass of the human **head and neck** target was 3.36 kg (7.41 pound), composed of the three component masses:

- The mass for the **brain and spinal cord** was 1.47 kg (3.24 pound).
- The mass for the **skull and neck** was 0.707 kg (1.56 pound).
- The mass for the **skin and muscles** was 1.19 kg (2.62 pound).

The initial position of the human **target** was placed in the center of the computational domain with room superior to the head to accommodate space for the downward-moving impactor. The centerline of the impactor cylinder was aligned to the centerline of the head, in the X- and Z-axes. The **impactor** was positioned vertically so that the bottom, exterior boundary of the padding layer was just superior to the crown of the head along the Y-axis.

The **impactor** had an initial velocity along the negative Y-axis with magnitude of 670, 1341, and 2012 cm s-1 (15, 30, and 45 mph), representing the three values chosen to parameterize the impact speeds. The **target** had quiescent initial velocity. Thus, the magnitude of the closing speeds between the two bodies equaled the initial speed of the impactor.

Symmetry along the vertical axis allowed a two-dimensional cylindrical domain to characterize the problem geometry. Four boundary conditions enclosed the computational domain, as shown in Figure 2-1. A symmetry boundary condition, which reflected normal incident pressure waves, ran along the central vertical axis of the impactor and target. Two outflow conditions, which allowed mass to leave but not enter, bounded the top and lateral extents of the domain. A transmitting condition, which allowed for inflow and outflow of mass, bounded the bottom of the domain near the base of the neck. The transmitting formulation modeled a semi-infinite medium, thus providing an inertial effect that would be generated on the neck by the torso.

Simulations were run in CTH,[10] an Eulerian, finite volume shock physics code developed and maintained by Sandia National Laboratories. A time history of 10-milliseconds was simulated, since it captured the impact pulse duration, typically around 6-milliseconds.

From the simulations, we obtained acceleration time histories at the center of mass of the head. Accelerations were filtered with a fourth-order, low-pass Butterworth filter with a cutoff frequency of 1650 Hertz.[1] The filtered acceleration time histories were then used to calculate the head injury criterion with a 6-millisecond time clip (HIC6).[12] The HIC, defined in Eq. (1),

$$\mathrm{HIC} = \left\{ (t_2 - t_1) \left[\frac{1}{t_2 - t_1} \int_{t_1}^{t_2} a(t)\, dt \right]^{2.5} \right\}_{\max} \qquad (1)$$

is calculated as an integral and power of the resultant head acceleration a and a function of time t, with time integration limits from t1 to t2, such that the HIC value is maximized.

3. RESULTS

Table 3-1 shows the Head Injury Criterion (HIC) results parameterized by impact speed and thickness.

Table 3-1. Head Injury Criterion (HIC) results parameterized by impact speed and padding thickness.

Impact Speed ($cm\ s^{-1}$)	Padding Thickness (cm)	Head Injury Criterion (HIC)
670	0	390
	1	103
	2	6.9
	4	3.1
	6	< 3
	8	< 3
	10	< 3
1341	0	1890
	2	1090
	4	498
	6	23.8
	8	13.9
	10	10.0
2012	4	2500
	6	1460
	8	835
	10	329

Figure 3-1 presents these same results, overlaid on probability of head injury curves as a function of HIC15. Three speeds were investigated, 670, 1341, and 2012 cm s^{-1} (15, 30, and 45 mph), which when combined with padding thicknesses from zero to 10 cm (3.9 inch), provided broad coverage of the AIS curves.

For the 17 simulations presented in Figure 3-1, the resulting head and neck deformation was essentially indistinguishable from the initial state shown in Figure 2-1. For completeness, we investigated an extreme case of an impactor, absent of padding, at 3353 cm s^{-1} (75 mph). This case, which produced a HIC value far exceeding 3000, demonstrated significant skull fracture profound brain extravasation, as shown in Figure 3-2.

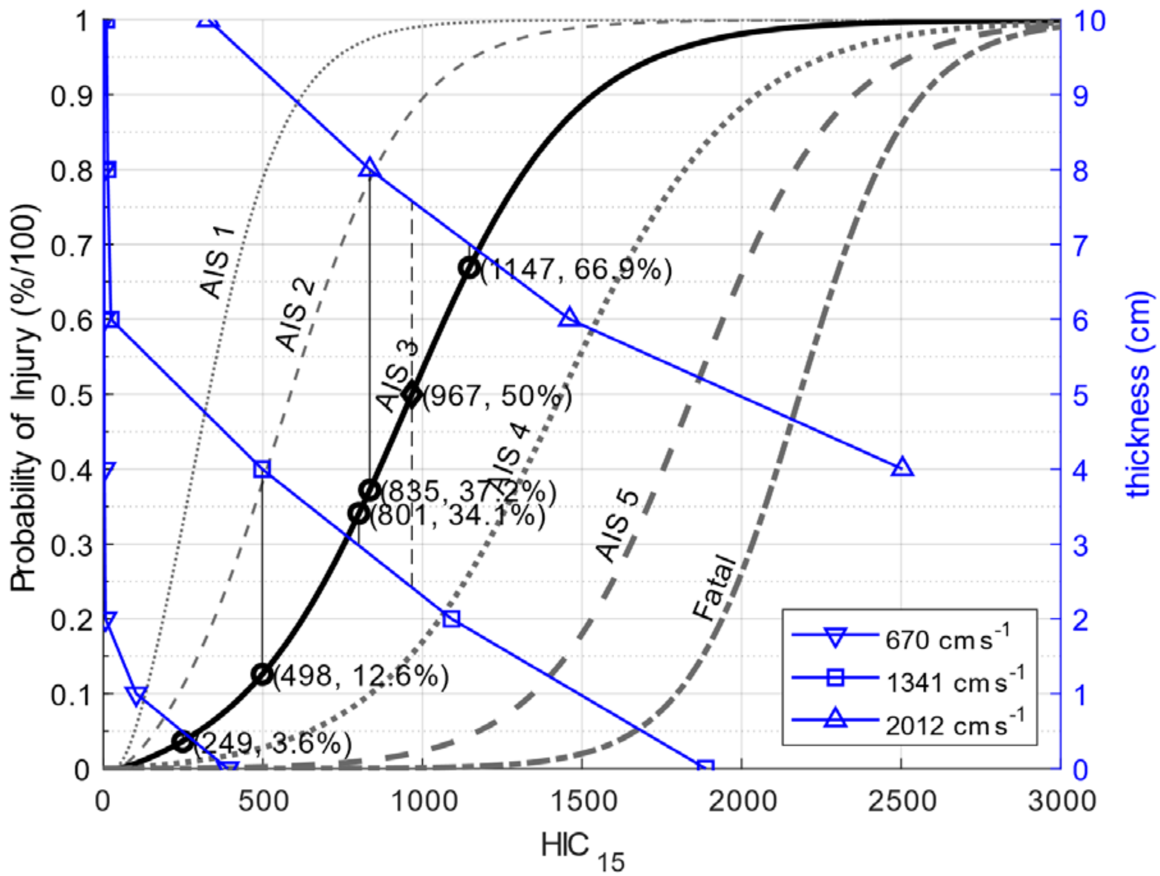

Figure 3-1. Head Injury Criterion (HIC) results for three speeds, 670, 1341, and 2012 cm s^{-1} (15, 30, and 45 mph), and padding thicknesses between zero and 10 cm (3.9 inch), mapped to the probability of injury AIS curves as a function of HIC. Key intercepts of interest, discussed in the text, are called out with circles, diamonds, and (HIC, injury probability) coordinates.

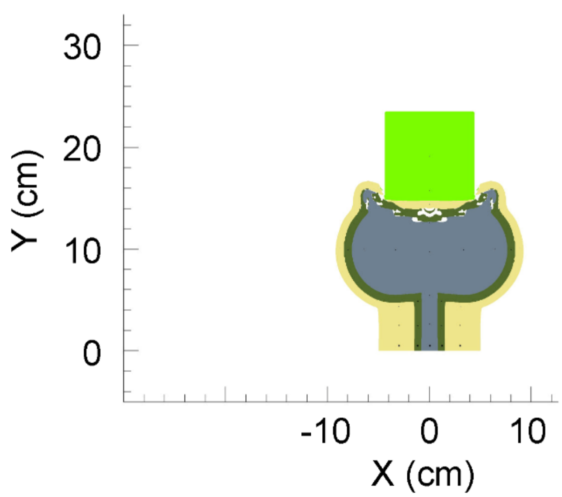

Figure 3-2. The impactor, without padding, with initial speed of 3353 cm s^{-1} (75 mph), causing catastrophic head impact at 1.0 millisecond after impact.

4. DISCUSSION

We chose our three initial conditions based upon impact speeds potentially observed during the service life of the subject balloon.[2]

- **Normal**: If the balloon were to land normally, the expected incident speed would be 581 cm s^{-1} (13 mph).
- **Complete Failure**: If the balloon experienced a complete dislocation from its payload, the expected incident speed would be 3353 cm s^{-1} (75 mph). This latter case could occur, for example, secondary to an in-flight collision event of the balloon with an aircraft.
- **Partial Failure**: Finally, we chose the intermediate value between normal operations and complete flight system failure as 1341 cm s^{-1} (30 mph). This incident speed represented a situation such as a tangled, partially inflated parachute.

These three speeds, 1341 cm s^{-1} (30 mph) plus/minus 670 cm s^{-1} (15 mph) provided broad coverage of the HIC domain (see Figure 3-1).

The 3353 cm s^{-1} (75 mph) case was to illustrate an outlier case, where gross deformations are so large, and results so catastrophic, that they are visible without magnification of the displacement state variables.

The choice of a 15-millisecond clip versus a 36-millisecond time interval in the calculation of HIC has been elucidated Eppinger et al.,[6] with emphasis on relatively long duration head impact events in automotive crashes, particularly with air bag deployments. Eppinger wrote, "The basis for AAMA's recommended 15 millisecond duration was that, in the original biomechanical skull fracture data from which HIC was derived, no specimen experienced a skull fracture and/or brain damage with a HIC duration greater than 13 milliseconds."

Indeed, in the 1985 work of Prasad and Mertz, the skull fracture group (n=54) had pulse durations ranging from 0.8 to 10.1-milliseconds and the brain damage group (n=25) ranged from 2.3 to 13.7-milliseconds.[16]

Our numerical experiments showed that head impact from balloon payload was a relatively short event, with impact durations on order of 10-millseconds or less. We elected to report all HIC values with a 6-millsecond time interval (HIC6), to assure the time interval was contained within the pulse duration of the impact. As noted by King, "...the limits of integration over time [are] selected so as to maximize with value of HIC. The time interval would obviously have to be within the pulse duration of the impact."[12]

We considered reporting HIC15, but found that for many cases, the pulse duration of the impact was significantly shorter than 15-millseconds. We thus elected HIC6, since the 6-millisecond time interval was spanned by impact event time durations.

Increasing padding thickness from zero resulted in reduction in HIC values, until HIC values asymptomatically approached zero. For example, for the 670 cm s^{-1} (15 mph), a 1 cm increase in padding thickness from zero resulted in a HIC reduction of 287, from 390 to 103. At this speed, an additional 1 cm (0.39 inch) increase up to 2 cm (0.79 inch) in padding thickness resulted in an additional HIC reduction of 96, from 103 to 6.9, approximately one-third of the previous HIC reduction when padding is increased from 0 to 1 cm (0.39 inch).

HIC reduction becomes less sensitive to increases in padding thickness as padding thickness increases from zero. This pattern, discussed above for the 670 cm s^{-1} (15 mph) was also observed for the two higher-speed cases, and can be seen graphically in Figure 3-1.

Figure 3 1 also shows a saturation thickness, which we define as a padding thickness beyond which no additional HIC reduction occurs. For the 670 cm s^{-1} (15 mph) case, the saturation thickness occurred at 2 cm (0.79 inch) thickness. For the 1341 cm s^{-1} (30 mph) case, the saturation thickness occurred at 6 cm (2.36 inch). For the 2012 cm s^{-1} (45 mph) case, we did not observe a saturation thickness, but a 10 cm (3.9 inch) padding thickness resulted in a HIC value of 329, which corresponded to probabilities of 50%, 18%, and 6% for AIS 1, AIS 2, and AIS 3 thresholds, respectively.

Padding provided meaningful reductions of injury risk outcomes at all speeds. The maximum risk of AIS 3+ injury was approximately 3.6% (HIC 249) for the 670 cm s^{-1} (15 mph) case with 0.5 cm (0.20 inch) of padding, 34% (HIC 801) for the 1341 cm s^{-1} (30 mph) case with 3.0 cm (1.2 inch) of padding, and 67% (HIC 1147) for the 2012 cm s^{-1} (45 mph) case with 7.0 cm (2.8 inch) of padding. Adding 1.0 cm (0.39 inch) of padding to these two latter cases reduced AIS 3+ injury risk to approximately 13% (HIC 498) and 37% (HIC 835), respectively. These intercepts are labeled on Figure 3 1.

Onset of AIS 3+ injury occurred for the 670 cm s^{-1} (15 mph) case when the padding was at approximately 0.5 cm (0.20 inch). For the 1341 cm s^{-1} (30 mph) case, AIS 3+ injury occurred when the padding was decreased to just over 3.0 cm (1.2 inch). Finally, for the 2012 cm s^{-1} (45 mph) case, AIS 3+ injury occurred at just below 7.0 cm (2.8 inch).

For the 1341 cm s^{-1} (30 mph) case, a padding thickness of less than 2.4 cm (0.94 inch) was more-likely-than-not AIS 3 injury producing. For the 2012 cm s^{-1} (45 mph) case, a padding thickness of less than 7.6 cm (3.0 inch) was more-likely-than-not AIS 3 injury producing. To achieve a less-likely-than-not outcome, padding at these two speeds should be 2.5 cm (0.98 inch) or greater and 8.0 cm (3.1 inch) or greater, respectively.

Practical application of the 1341 cm s^{-1} (30 mph) case suggest that 5.0 cm (2.0 inch) padding thickness guards against injury, with HIC values of approximately 260, which corresponds to AIS 3+ injury risk of 3.9%. The 5.0 cm (2.0 inch) value appears to make probability of AIS 3+ injury less-likely-than-not up to approximately 1676 cm s^{-1} (37.5 mph), near approximate midcourse between the 1341 cm s^{-1} (30 mph) and 2012 cm s^{-1} (45 mph) curves.

Balloon operators may use the foregoing risk analysis with additional data describing the probability of a failure mode to occur to construct conditional probability injury risk assessments. For example, while the probability of AIS 3+ injury with 5 cm (2 inch) of padding and impact speed of 1341 cm s^{-1} (30 mph) was found to be 3.9%, the actual risk of this injury outcome is significantly less once conditional probability of having a 1341 cm s^{-1} (30 mph) event is considered. Further injury risk reductions would be expected if conditional probabilities of having a human in the descent path of the falling payload were incorporated. Flight paths over population centers would maximize this conditional probability; over rural-to-uninhabited geographies would minimize this conditional probability.

One recent study characterized injury risk to a Hybrid III test device from three commercially-available unmanned aircraft systems (UAS) with mass ranging from 1.2 kg (2.6 pound) to 11 kg (24 pound) and impact speeds ranging from 1600 cm s^{-1} (35.8 mph) to 2200 cm s^{-1} (49.2 mph).[3] Of all their experiments, the falling impact test (n=7) of the DJI phantom 3 --- with mass of 1.2 kg (2.6 pound), impact speed of 1000 cm s^{-1} (22.4 mph), and HIC15 of 12 (median) and 2-12 (interquartile range) --- would most closely match our model, with weight of 1.5412 kg (3.40 pound) at 670 cm s^{-1} (15 mph) with 2 cm (0.79 inch) padding (HIC 6.9). Their research noted that the UAS leg struck the top of the head and then deformed, causing the UAS velocity to be "greatly reduced" prior its body contacting the head. We interpret this kinetic energy reduction through UAS leg deformation as similar in mechanism to our padding.

While our work presents a comprehensive analysis of falling balloon payloads at a range of impact speeds and protective foam padding thicknesses, it represents the worst-case head impact scenario: A perfectly aligned vertical impact with all the kinetic energy from the impactor directed into the target. In this context, then, we interpret the results herein as an upper bound.

In field events, we would rarely expect such perfect vertical alignment of the impactor with the target. Indeed, as seen in Campolettano et al.,[3] where the articulations move and pivot the main mass away from the head after initial contact, and thus reduce injury to the head, we envision our impactor tumbling (rotation) in addition to falling (translation). This rotation, in conjunction with unlikely nature of perfect impactor-to-target alignment on contact, would cause the impactor to contact yet tumble away from the head upon rebound.

Our work explored the impact configuration where the payload presents a blunt surface to the crown of the head. We did not explore presentation to the head with a payload corner. Given this alternate configuration, we would anticipate that at relatively slower impact speeds, the corner would act as a fulcrum, pivoting and redirecting the payload prior to padding crush up. Conversely, at relatively higher speeds, we would expect padding crush up prior to significant redirection, and a penetrating skull fracture to result. If these corner impact configuration prognostications were found to be true, an interesting avenue for future work, it may suggest payloads with a spherical geometry, rather than cubic or cylindrical geometry, may further help to reduce injury risk.

5. CONCLUSIONS

We have quantified injury risk by way of the head injury criterion (HIC) to humans on the ground, subject to head impact from a falling balloon payload. We parameterized impactor speed and padding thickness to provide wide coverage of the injury risk curves. This analysis should help balloonists specify padding safeguards and serve as a basis for their own comprehensive risk assessments. Operators should use padded payload boxes and include a descent arrestor system, such as a parachute, to decrease the deleterious consequences of possible impacts from payload to humans on the ground.

REFERENCES

[1] Alem, N. and M. Perry. Design of digital low-pass filters for time-domain recursive filtering of impact acceleration signals. USAARL Report No. 95-13. United States Army Aeromedical Research Laboratory, 1995.

[2] Bowman, D.C. Analysis of the Heliotrope flight system failure on May 29, 2015. *Technical report SAND2018-3465*, Sandia National Laboratories, Albuquerque NM USA, 2018.

[3] Campolettano, E.T., M.L. Bland, R.A. Gellner, D.W. Sproule, B. Rowson, A.M. Tyson, S.M Duma, and S. Rowson. Ranges of injury risk associated with impact from unmanned aircraft systems. *Ann. Biomed. Eng.* 45(12):2733-2741, 2017.

[4] Code of Federal Regulations, Title 14, Chapter I, Subchapter F, Part 101 – Moored balloons, kites, amateur rockets, unmanned free balloons, and certain model aircraft.

[5] Eggers, J. Update on BETTII Mission Flight Termination, Recovery. Retrieved from https://www.nasa.gov/feature/wallops/2017/update-on-bettii-mission-flight-termination-recovery. June 11, 2017.

[6] Eppinger R., E. Sun, F. Bandak, M. Haffner, N. Khaewpong, M. Maltese, S. Kuppa, T. Nguyen, E. Takhounts, R. Tannous, and A. Zhang. Development of improved injury criteria for the assessment of advanced automotive restraint systems–II. National Highway Traffic Safety Administration. 5:1-70, November 1999.

[7] Gaskin, J.A., I.S. Smith, and W.V. Jones. Introduction to the Special Issue on Scientific Balloon Capabilities and Instrumentation. *J. Astronom. Instrum.* 3(2):1403001-1-18, 2014.

[8] Google Project Loon. Retrieved from https://x.company/loon/. March 21, 2018.

[9] Hallquist, J.O. LS-DYNA theory manual. Livermore software technology corporation, Mar, 2006, p20.2.

[10] Hertel, E.S., R.L. Bell, M.G. Elrick, A.V. Farnsworth, G.I. Kerley, J.M. McGlaun, S.V. Petney, S.A. Silling, P.A. Taylor, and L. Yarrington. CTH: A software family for multi-dimensional shock physics analysis. In *Shock Waves@ Marseille I*. Springer, Berlin, Heidelberg, 1995, pp. 377-382.

[11] Johnson, G.R. and W.H. Cook Fracture characteristics of three metals subjected to various strains, strain rates, temperatures and pressures. *Eng. fract. mech.* 21(1):31-48, 1985.

[12] King, A.I. Basics of the Biomechanics of Brain Injury. In *The Biomechanics of Impact Injury*. Springer, Cham, 2018, pp. 35-76.

[13] Lyon, S. P., and J. D. Johnson. T-1 handbook of the SESAME equation of state library. Los Alamos National Laboratory, Los Alamos, NM, LA-CP-98-100, 1998.

[14] NASA Eclipse Ballooning Project. Retrieved from https://eclipse2017.nasa.gov/. August 21, 2017.

[15] Olsen, E.M., J. T. Rosenberg, J. D. Kawamoto, C. F. Lin, and L. Seaman. XDT Investigations by computational simulations of mechanical response using a new viscous internal damage model. In *Eleventh Symposium (International) on Detonation*. 1998, pp. 170-178.

[16] Prasad, P. and H.J. Mertz. The position of the United States delegation to the ISO Working Group 6 on the use of HIC in the automotive environment (No. 851246). SAE Technical Paper, 1985.

[17] Shaw, W.N. Léon Phillippe Teisserence De Bort. *Nature.* 90(2254):519-520, 1913.

[18] Taylor, P.A., J.S. Ludwigsen, and C.C. Ford. Investigation of blast-induced traumatic brain injury. *Brain injury*. *28*(7):879-895, 2014.

[19] Walker, J.D. Impact modeling. In *Report of the Columbia Accident Investigation Board.* Vol. 2. Appendix D.12. U.S. Government Printing Office, Washington D.C., October 2003, pp. 360-390.

[20] Yajima, N, N. Izutsu, T. Imamura, and T. Abe. *Scientific Ballooning: Technology and Applications of Exploration Balloons Floating in the Stratosphere and the Atmospheres of Other Planets.* Vol. 112. Springer Science& Business Media, 2009.

APPENDIX A. REPRESENTATIVE CTH INPUT FILE

```
************************************************************
*
*     20180106 CBH
*     parent is sim_075_01t_H01.i
*     2-D cth calculations of canister impact to the head
*
*************************************************************
*
*eor* cthin
*
*************************************************************
*
Canister Impact
*
*restart
*  time=1.13e-2
*endrestart
*
control
  mmp0
*  nscycle = 0 * test diatom setup, least compute time
*  nscycle = 1 * test solve, small compute time
*  tstop = 15.0e-3 * seconds
   tstop = 10.0e-3 * seconds
*
*  dtcourant = 0.3 * 20180118 based on Arne Gullerud suggestion
endc
*
mesh
*
  block 1  geom=2dc  type=e
*
    x0 0.0
     x1 dxf=0.10 dxl=0.10 w=19.0
    endx
*
    y0 0.0
     y1 dyf=0.10 dyl=0.10 w=51.0
    endy
*
  endb
*
endmesh
*
spy

 Save("VOLM,M,P,VX,VY,XXDEV,XYDEV,YYDEV,DMG2,EM+1,EM+2,EM+3"); SaveTime(0,10.e-5);
 SaveHis("POSITION,VX,VY,VZ,P"); HisTime(0,1.e-5);
 SaveTracer(ALL);
endspy
*
****************************************************************
* material insertion inputs

diatom
    package 'Brain-1'
     iter 4
     material 1
*     pressure 1.e6
```

```
     insert circle
       ce = 3.10, 10.5 * Vol=1406.2cc
       ra = 4.7
     endinsert
     insert box
       p1 =   0.0,  0.0
       p2 =   0.8,  5.8
     endinsert
     insert box
       p1 =   0.0,   5.8
       p2 =   3.10, 15.2  * Vol=1406.2cc
     endinsert
    endpackage

    package 'Skull-1'
     iter 4
     material 2
*     pressure 1.e6
     insert circle
       ce = 3.10, 10.5
       ra = 5.5
     endinsert
     insert box
       p1 = 0.0,  0.0
       p2 = 1.5,  5.0
     endinsert
     insert box
       p1 = 0.0,  5.0
       p2 = 3.10, 16.0
     endinsert
    endpackage

    package 'skin-muscle'
     iter 4
     material 3
*     pressure 1.e6
     insert box
       p1 =   0.0,  0.0
       p2 =   5.0,  5.0
     endinsert
     insert box
       p1 =   0.0, 16.0
       p2 =   3.10, 16.8
     endinsert
     insert circle
       ce = 3.10, 10.5
       ra = 6.3
     endinsert
    endpackage

*    package 'Sensor Technology'
** need to specify*
*     iter 4
*     material 4
*     yvel=-1341.12
**     pressure 1.e6
*     insert box
*       p1 =
*       p2 =
*     endinsert
*    endpackage
```

```
    package 'Aluminum'
*need to change material properties. Geometry is correct*
     iter 4
     material 5
     yvel=-1341.12
*    yvel =  -581.152 * cm/s = 13 mph
*    yvel = -1341.12  * cm/s = 30 mph
*    yvel = -3352.79  * cm/s = 75 mph
*     pressure 1.e6
     insert box
       p1 =   0.0, 18.8
       p2 =   4.4958, 27.7916
     endinsert
    endpackage

    package 'Styrofoam Box'
*need to change material properties. Geometry is correct*
     iter 4
     material 6
     yvel=-1341.12
*    yvel =  -581.152 * cm/s = 13 mph
*    yvel = -1341.12  * cm/s = 30 mph
*    yvel = -3352.79  * cm/s = 75 mph
*    pressure 1.e6
     insert box
       p1 =   0.0,    16.8
       p2 =   6.4958, 29.7916
     endinsert
    endpackage

enddiatom

****************************************************************
*
tracer
 block 1
* Tracers in brain:
   add 0.0 15.0                    *Pt.1; Crown of Brain
   add 0.0 10.5  to 6.5 10.5  n=3  *Pt.2-4; Horizontal midline of Brain
   add 0.0  5.5                    *Pt.5; Base of Brain
   add 0.0  2.5                    *Pt.6; Mid Brain Stem
   add 0.0  0.5                    *Pt.7; Base of Brain Stem
* Tracers in bone:
   add 0.0 15.6                    *Pt.8; Crown of Skull
   add 8.2 10.5                    *Pt.9; Temporal side of Skull
   add 1.2  5.0                    *Pt.10; Base of Skull
   add 1.2  2.5                    *Pt.11; Mid-height of neck bone
   add 1.2  0.5                    *Pt.12; Base of neck bone
* Tracers in scalp:
   add 0.0  16.4                   *Pt.13; Crown of Scalp
   add 9.0  10.5                   *Pt.14; Temporal side of Scalp
   add 3.0  4.5                    *Pt.15; Top of neck tissue
   add 3.0  2.5                    *Pt.16; Mid-height of neck tissue
   add 3.0  0.5                    *Pt.17; Base of neck tissue
* Tracers in Foam:
   add 0.0  17.8                   *Pt.18; Center of Foam Buffer
* Tracer in the Al block:
   add 0.0 23.2958              *Pt.19; center of the aluminum block
 endb
endtracer
```

```
*
eos

* eosfile='/home/pataylo/cth9.1/Mod2/cth/data/EOS_data'
*  -----------------------
*  Mie-Gruneisen Brain (pat 4/17/95) (both wm & gm use same eos representation)
*  -----------------------
* WM:
  mat1  mgr user     g0=1.0    cs=1.51e5    cv=1.0e10
        r0=1.040     s1=1.409

*  -----------------------
*  Mie-Gruneisen Bone
*  -----------------------
  mat2  mgr user        g0=1.0          cs=1.9838e5     cv=1.0e10  *New Values
        r0=1.210        s1=1.0                                     *New Values

*  -----------------------
*  Mie-Gruneisen Scalp & Muscle (need to replace this with more accurate representation)
*  -----------------------
  mat3  mgr user    g0=1.0    cs=1.703e4    cv=1.0e10  * r0*cs^2 = 34.8 MPa
        r0=1.20     s1=1.0

*  -----------------------
*  Sticky Fill (Sesame Water)
*  -----------------------
  mat4 ses water
           sr=0.91743  *initial density = 1.09 g/cc

*  -----------------------
*  Canister (Sesame Al)
*  -----------------------
  mat5 ses aluminum

*  -----------------------
*  Foam Buffer (Sesame ?)
*  -----------------------
  mat6 foam ncfi24-124

endeos
*  ---
*  -----------------------
*  ---
epdata

*fvp='/home/pataylo/cth9.1/Mod2/cth/data/VP_data'

*Brain_GM:
  matep 1   vep=user
             gsi=1.04
             g0=6.4e4
             g1=27.6e4
             amu1=6900.  *from Ludwigsen's match to Bayly's MRI Elastography data (relax
time=25ms)
*             amu1=394.2857  *from Zhang, Yang, & King
             phism=0.1
             nmax=1
             poisson=0.49

*Skull:
  matep 2 EPPVM user  yield=0.95e9  poisson=0.22
```

```
            jfrac=user    jfpf0=-0.775e9   jfd1=0.008   jfd2=0
            jfd3=0        jfd4=0           jfd5=0       jftm=1.e20

*Scalp & Muscle: (Keep response elastic)
  matep 3  EPPVM user  yield=1.e8   poisson=0.42  * Increase strength to eliminate scalp spall
(Frt/10h3)

*Al Canister
  matep 5  jo 6061-t6_aluminum  poisson=0.33  *

*Foam Buffer
  matep 6  jo user  *Foam insulation model created by J.Walker for Shuttle work (2003)
              ajo=9.2e6 * dyne/cm^2 = 0.920 MPa, formerly 7.e7  dyne/cm^2
             bjo=0. * hardening
             njo=1. * hardening exponent
             cjo=0.0 * strain rate dependence
             mjo=1. * homologous temperature exponent
             tjo=1. * same as tmelt
              tmelt=1. * same as tjo
              poisson=0.2 * formerly 0.0

  esav    * Save Isotropic & Deviatoric Strain Energies

  lstrain * Calculate and save Lagrangian Strain Tensor

  mix 5
endep

extremum
 dyn
  maximum
    pressure
    vmst    * von Mises stress
  *  edse    * deviatoric strain energy
  *  eisr    * isotropic strain energy
*
  minimum
    pressure
endext

cellthermo
  mmp0
  tbad=100000000000
endcell

convct
  convection=0
  interface=smyra
endconv

fracts
  pressure
*  stress
  pfrac1 -0.1e9   *GM
  pfrac2 -0.775e9 *Skull
  pfrac3 -0.1e9   *Scalp/Muscle; Increase to eliminate spalling of skin (Frt/10h2, Side/2b &
2b2)
  pfrac4 -0.9e6   *Water
  pfrac5 -3.1e9   *6061-T6 Aluminum
  pfrac6 -2.3e6   *Foam buffer (from J.Walker report on Foam model)
  pfmix  -1.e20
```

```
  pfvoid -1.e20
endfrac

edit

  shortt
    time=0.  dt=10.
  ends

  longt
    time=0.  dt=10.
  endl

  plotdata
   plt
    mass
    volume
    pressure
    stress
    energy
    extra
  endplot

  plott
    time=0.       dt=20.0e-6
  endp

  restt
    time=0.  dt=100.e-6
  endr

  histt
    time=0.  dt=1.0e-6
    htracer all
  endh

ende

boundary
  bhydro
    block 1
      bxbot=0     bxtop=2.1    *X-bottom reflective & X-top flow-through
      bybot=1     bytop=2.1    *Y-bottom SS absorbing & Y-top flow-through
*      bybot=2.1   bytop=2.1    *Y-bottom & Y-top flow-through
    endblock
  endhydro
endboundary
*
discard

*  Discard all mats on negative temps
    mat=-1 temp=0. dens=100.
*  Discard all mats on negative energy
    mat=-1 enrg=0. dens=100.
*  Discard all mats on low density (1% of reference)
    mat=-1 dens=-0.01

enddiscard
*
mindt
  time=0. dt=1.e-10
```

```
endmin
*
*******************************************************************
*eor* pltin
*******************************************************************
*
catalog
units,cgsk
color, table=3
*color,frame=7,if=7
left,if,bands
right,if,bands
flegend,bands
limits,x=-10.0,10.0,10  y=-10.0,10.0,10
time=1.e-6, rest
*
title, Pressure
rbands,b1=-30.e6,b2=40.e6,c1=207,c2=16,cs=207,ce=16
2dplot,if,bands=pressure
*
title, Deviatoric Stress Magnitude
rbands,b1=1.e6,b2=40.e6,c1=207,c2=16,cs=0,ce=7
2dplot,if,bands=j2p
*
*******************************************************************
```

DISTRIBUTION

Email—Internal

Name	Org.	Sandia Email Address
Stephen Warner	0622	swarner@sandia.gov
Marilyn S. Bange	0632	msbange@sandia.gov
John E. Myers	0632	jemyers@sandia.gov
Taffey Jo Miller	0637	tmaddox@sandia.gov
Ramon Reyes	1542	rreyes@sandia.gov
Marcus J. Martinez	5410	martimj@sandia.gov
Dennis R. Helmich	5420	drhelmi@sandia.gov
Candice F. Cooper	5421	cfcoope@sandia.gov
Douglas A. Dederman	5421	dadeder@sandia.gov
Shivonne Haniff	5421	shaniff@sandia.gov
Chad B. Hovey	5421	chovey@sandia.gov
Ryan J. Terpsma	5421	rjterps@sandia.gov
Kevin P. Ruggigello	5421	kruggir@sandia.gov
Jonathan B. Christensen	5422	jbchris@sandia.gov
Daniel Bowman	6752	dbowma@sandia.gov
Technical Library	9536	libref@sandia.gov

This page left blank

This page left blank

Sandia National Laboratories

Sandia National Laboratories is a multimission laboratory managed and operated by National Technology & Engineering Solutions of Sandia LLC, a wholly owned subsidiary of Honeywell International Inc. for the U.S. Department of Energy's National Nuclear Security Administration under contract DE-NA0003525.